

Simulating Electromagnetic Cascades with Lorentz Invariance Violation

Andrey Saveliev^{1,2}, Rafael Alves Batista^{3,4,5}

¹Immanuel Kant Baltic Federal University, Ul. A. Nevskogo 14, Kaliningrad, Russia

²Lomonosov Moscow State University, GSP-1, Leninskiye Gory 1-52, Moscow, Russia

³Instituto de Física Teórica UAM-CSIC, Universidad Autónoma de Madrid, C/ Nicolás Cabrera 13-15, 28049 Madrid, Spain

⁴Departamento de Física Teórica, Universidad Autónoma de Madrid, M-15, 28049 Madrid, Spain

⁵Sorbonne Université, CNRS, UMR 7095, Institut d'Astrophysique de Paris, 98 bis bd Arago, 75014 Paris, France

E-mail: andrey.saveliev@desy.de, rafael.alves_batista@iap.fr

Abstract.

Lorentz invariance violation (LIV) is a phenomenon featuring in various quantum gravity models whereby Lorentz symmetry is broken at high energies, potentially impacting the behaviour of particles and their interactions. Here we investigate the phenomenology of LIV within the context of gamma-ray-induced electromagnetic cascades. We conduct detailed numerical simulations to explore the expected manifestations of LIV on gamma-ray fluxes, taking into account relevant effects such as pair production and inverse Compton scattering. Additionally, we consider processes forbidden in the Standard Model, namely vacuum Cherenkov emission and photon decay. Our analysis reveals that these modifications result in distinct characteristics within the measured particle fluxes at Earth, which have the potential to be observed in high-energy gamma-ray observations.

Contents

1	Introduction	2
2	Particle Propagation with Modified Dispersion Relations	4
2.1	Modified Thresholds for Electromagnetic Interactions	4
2.2	New Electromagnetic Processes	5
3	Simulations of Electromagnetic Cascades with Lorentz Invariance Violation	8
3.1	Simulations: Photon Propagation	10
3.2	Simulations: Electron Propagation	10
3.3	Simulations: Full LIV Phenomenology	11
3.4	Simulations: Effects of the Intrinsic Properties of the Source	12
4	Discussion	13
5	Conclusions and Outlook	15

1. Introduction

The Standard Model (SM) of particle physics is a highly successful theory that provides an elegant description of three out of the four known fundamental forces of nature, namely electromagnetic, weak, and strong interactions, leaving aside only gravity [1, 2]. A unified theory describing these four forces – if it exists – would completely transform our understanding of nature and is arguably one of the most important problems in fundamental physics.

The SM has proven remarkably effective in explaining a wide array of physical phenomena. Nevertheless, several unresolved issues persist, stemming from both experimental observations and theoretical considerations. These include phenomena like dark matter, dark energy, neutrino masses, and the hierarchy problem [3].

Quantum gravity (QG) theories attempt to describe the four fundamental forces within a single theoretical framework [4]. It generally strives to bridge the gap between the quantum field theory approach of the SM and the differential geometry framework employed in general relativity (GR). This task presents a significant challenge due to the classical nature of GR, which inherently complicates its combination with any form of quantization.

QG is expected to manifest itself only at high energies, comparable to the Planck mass ($M_{\text{Pl}} \simeq 1.22 \times 10^{28}$ eV) – otherwise it would probably have already been detected in particle accelerators, whose maximal attainable energy is more than a dozen orders of magnitude below M_{Pl} . Over very long baselines, Planck-scale effects can be magnified and lead to a measurable signal, as is the case of high-energy particles propagating over

cosmological distances [4], such as ultra-high-energy cosmic rays (UHECRs) [5, 6, 7] and very-high-energy gamma rays [5, 8, 9].

There have been several works positing that QG lead to a phenomenon known as Lorentz invariance violation [10, 11, 12, 13, 14]. Lorentz symmetry can be broken if at least one of the pillars upon which it rests is broken, namely the principle of relativity, which ensures the equivalence of the laws of physics in all inertial frames, or the constancy of the speed of light. The immediate phenomenological consequence of LIV is, thus, a modification of the energy-momentum dispersion relation and spatio-temporal changes. Note that some QG frameworks also feature modified dispersion relations whilst merely deforming Lorentz symmetry. This, for example, is the case for deformed (or doubly) special relativity (DSR) [15, 16].

While there are currently no compelling hints of LIV, it could either be small or manifest itself at energies beyond current observational limits. Therefore, attempts to perform experimental searches for LIV often employ an effective field theoretical framework, like SM extensions [10], whose operators directly translate into *measurable* phenomenological observables such as energy-dependent time delays [17, 18, 19, 20, 21] and anomalous interaction thresholds [22, 23, 24, 25, 7, 26] (see [4] for a comprehensive review).

In this work we focus on the expected signatures of LIV on gamma rays from cosmological sources, considering their intergalactic propagation [27]. During their journey from an astrophysical object to Earth, sufficiently energetic photons from an astrophysical object like a blazar or a gamma-ray burst interact with radiation pervading the universe, such as the cosmic microwave background (CMB) and the extragalactic background light (EBL), producing an electron-positron pair. These pairs, in turn, interact with background photons via inverse Compton scattering, transferring a substantial fraction of their energy to the photons resulting from it. These photons, depending on their energy, can trigger these interactions yet again, until the high-energy photons no longer have sufficient energy to start the reaction. Therefore, a single primary photon of sufficiently high energy can result in copious amounts of secondaries, tertiaries, and higher-order gamma rays. This energy *threshold* is modified if LIV is acting [28, 22], changing the interaction length for pair production and igniting or quenching the cascade.

In this work, we perform Monte Carlo simulations of the development of electromagnetic cascades, considering the modified dispersion relations that affect very-high-energy (VHE) photons and electrons during their propagation. To this end, we begin in Sec. 2 by introducing the formalism governing the propagation of electrons and positrons, emphasising modifications stemming from the modified dispersion relations. Subsequently, in Sec. 3, we outline the simulation setup for the electromagnetic cascades incorporating LIV effects and present the corresponding simulation results. In Sec. 4 we discuss our findings and the implications for searches of LIV using high-energy gamma-ray observations. Lastly, in Sec. 5 we draw our conclusions and briefly address the issue of employing this strategy for LIV studies.

2. Particle Propagation with Modified Dispersion Relations

The aforementioned dispersion relations relevant for electromagnetic cascades are in general given by [29]

$$E_e^2 = p_e^2 \left[1 + \frac{m_e^2}{p_e^2} + \sum_{j=0}^N \chi_j^e \left(\frac{p_e}{M_{\text{Pl}}} \right)^j \right], \quad (1)$$

$$E_\gamma^2 = k_\gamma^2 \left[1 + \sum_{j=0}^N \chi_j^\gamma \left(\frac{k_\gamma}{M_{\text{Pl}}} \right)^j \right] \quad (2)$$

for electrons/positrons and photons, respectively. Here, m_e is the electron mass, while p_e and k_γ is the electron and photon momentum, respectively. On the other hand, χ_j^γ and χ_j^e are the corresponding LIV parameters of the j th order.

Usually one assumes that one of the terms of the sums (of order $n = 0, 1, 2, \dots$) present in Eqs. (1) and (2) is dominant, such that these equations may be reduced to

$$E_e^2 = p_e^2 \left[1 + \frac{m_e^2}{p_e^2} + \chi_n^e \left(\frac{p_e}{M_{\text{Pl}}} \right)^n \right], \quad (3)$$

$$E_\gamma^2 = k_\gamma^2 \left[1 + \chi_n^\gamma \left(\frac{k_\gamma}{M_{\text{Pl}}} \right)^n \right], \quad (4)$$

respectively. In case of $\chi_n^i < 0$ the corresponding LIV scenario is also called subluminal, while for $\chi_n^i > 0$ it is denoted as superluminal. Evidently, $\chi_n^i = 0$ reduces to the usual case of special relativity (SR).

The consequences of these modifications are two-fold [22]. Firstly, the threshold of a given reaction is altered, leading to a modification in the associated propagation length, as described in Sec. 2.1. Secondly, the presence of LIV enables new reactions that would otherwise not be possible within the confines of Lorentz invariance. Examples of such reactions include the spontaneous decay of photons into pairs or photons, as well as the occurrence of the vacuum Cherenkov effect for electrons, both described in Sec. 2.2.

2.1. Modified Thresholds for Electromagnetic Interactions

Here, we primarily consider the threshold modification. In order to calculate the threshold of a given reaction, one has to solve the equation

$$\max_{0 \leq \theta \leq \pi} s^{\text{in}}(\theta) = \min_{0 \leq y \leq 1} s^{\text{out}}(y), \quad (5)$$

where $s^{\text{in}}(\theta)$ and $s^{\text{out}}(y)$ is the invariant mass of the incoming and outgoing particles, respectively, given by the symbolic reaction equations

$$\gamma_{\text{HE}} + \gamma_{\text{bg}} \rightarrow e_{\text{HE}}^+ + e_{\text{HE}}^- \quad (6)$$

for pair production, and

$$e_{\text{HE}}^\pm + \gamma_{\text{bg}} \rightarrow e^\pm + \gamma_{\text{HE}} \quad (7)$$

for inverse Compton scattering, where in both cases γ_{bg} denotes a background photon, while e_{HE}^{\pm} and γ_{HE} is a high-energy (HE) electron/positron and photon, respectively. The maximum on the left side of the equation should be searched regarding the angle θ between the propagation directions of the two incoming particles. On the other hand, since the directions outgoing particles for very high energies may be regarded as nearly parallel, the minimum on the right hand side should be searched regarding the fraction y of the total energy carried by one of the outgoing particles.

This results in the background photon threshold energy, ϵ_{thr} , given by

$$\epsilon_{\text{thr}} = \begin{cases} k_{\gamma} \left[\left(\frac{m_e}{k_{\gamma}} \right)^2 + \frac{1}{4} \left(\frac{\chi_n^e}{2^n} - \chi_n^{\gamma} \right) \left(\frac{k_{\gamma}}{M_{\text{Pl}}} \right)^n \right] & \text{for pair production,} \\ 0 & \text{for inverse Compton scattering,} \end{cases} \quad (8)$$

or, equivalently, in the threshold invariant mass, s_{thr} , which may be written as

$$s_{\text{thr}} = \begin{cases} k_{\gamma}^2 \left[4 \left(\frac{m_e}{k_{\gamma}} \right)^2 + \frac{\chi_n^e}{2^n} \left(\frac{k_{\gamma}}{M_{\text{Pl}}} \right)^n \right] & \text{for pair production,} \\ p_e^2 \left[\left(\frac{m_e}{p_e} \right)^2 + \chi_n^e \left(\frac{p_e}{M_{\text{Pl}}} \right)^n \right] & \text{for inverse Compton scattering.} \end{cases} \quad (9)$$

Using these results, one then can calculate the mean free path λ by [4]

$$\lambda^{-1} = \frac{1}{2p_{\text{in}}} \int_{s_{\text{thr}}}^{\infty} \frac{n_{\text{bg}} \left(\frac{s^* - \mathfrak{S}(p_{\text{in}})}{4p_{\text{in}}} \right)}{[s^* - \mathfrak{S}(p_{\text{in}})]^2} \int_{\mathfrak{S}(p_{\text{in}})}^{s^*} \sigma(s) [s - \mathfrak{S}(p_{\text{in}})] ds ds^*, \quad (10)$$

where p_{in} , m_{in} and χ_n^{in} is the momentum, mass and LIV parameter of the incoming VHE particle, respectively, $n_{\text{bg}}(\epsilon)$ is the ambient photon density of the background photon field, and $\sigma(s)$ is the cross section of the considered reaction, while s_{thr} is given by Eq. (9) and $\mathfrak{S}(p_{\text{in}})$ by

$$\mathfrak{S}(p_{\text{in}}) \equiv p_{\text{in}}^2 \left[\left(\frac{m_{\text{in}}}{p_{\text{in}}} \right)^2 + \chi_n^{\text{in}} \left(\frac{p_{\text{in}}}{M_{\text{Pl}}} \right)^n \right]. \quad (11)$$

In Fig. 1 we show some examples of mean free paths for pair production by gamma rays according to Eq. (10). Fig. 2 illustrates the same scenarios considering inverse Compton scattering.

2.2. New Electromagnetic Processes

In addition, we also take into account the most important “new” reactions, i.e. reactions which are only possible when Lorentz invariance is violated: the vacuum Cherenkov effect and photon decay.

The phenomenon known as vacuum Cherekov effect can be described by the spontaneous emission of a photon by a massive particle, in this case, electrons and positrons. This is represented by the reaction

$$e^{\pm} \rightarrow e^{\pm} + \gamma, \quad (12)$$

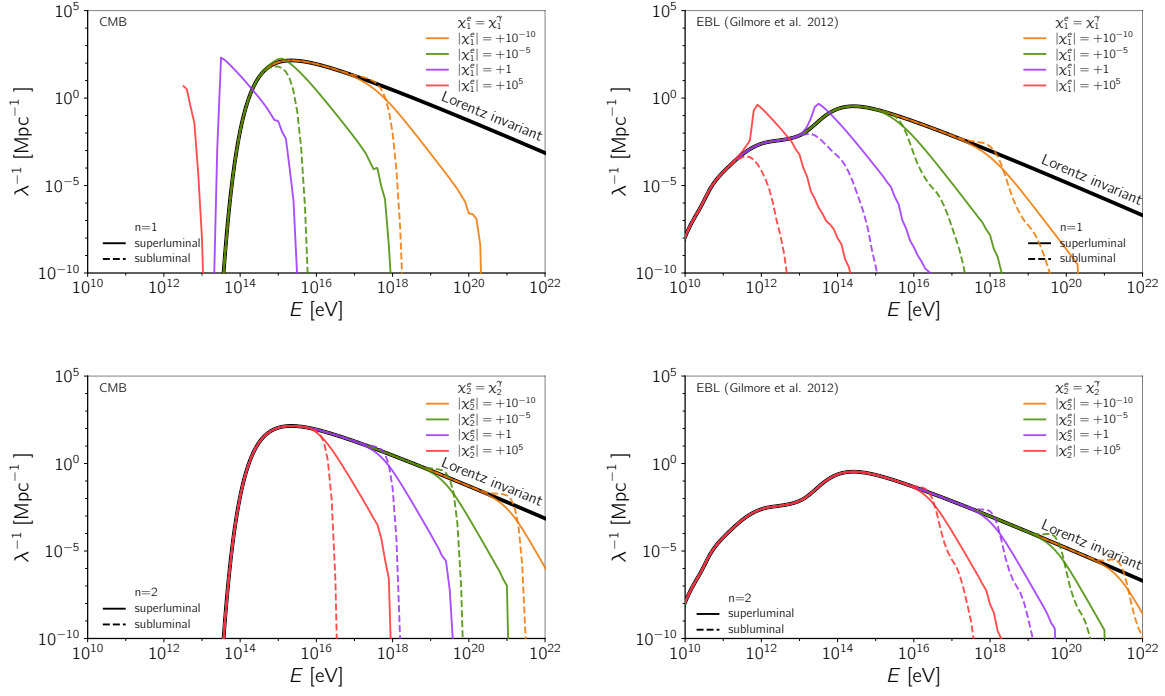


Figure 1. Examples of mean free paths for pair production including LIV calculated according to Eq. (10). The left panel corresponds to the CMB, whereas the right one corresponds to the EBL model from [30]. The upper panels depict the case of first order LIV, whereas the lower ones are for second order LIV. The LIV parameters for each case are indicated in the legend.

Within our framework, we make the assumption that if the parent’s energy exceeds the threshold for vacuum Cherekov (VC), it will emit one or more photons until its energy falls below this threshold. To streamline our approach, we adopt a “binary” methodology: if the electron or positron’s energy is *above* the threshold, we reduce its energy to match the threshold value. Conversely, if the energy falls *below* the threshold, we do not consider the VC effect. This evaluation is conducted at each propagation step. The specific threshold value we utilize is derived from the findings presented in [22], which we summarize in the following section.

For $n = 0$ we get the threshold value

$$p_{\text{thr}}^{\text{VC}} = \begin{cases} \frac{m_e}{(\chi_0^e - \chi_0^\gamma)^{\frac{1}{2}}} & \text{for } \chi_0^e > \chi_0^\gamma, \end{cases} \quad (13)$$

while for $n = 1$ we have

$$p_{\text{thr}}^{\text{VC}} = \begin{cases} \left(\frac{m_e^2 M_{\text{Pl}}}{2\chi_1^e} \right)^{\frac{1}{3}} & \text{for } \chi_1^e > 0 \text{ and } \chi_1^\gamma \geq -3\chi_1^e, \\ \left[-\frac{4m_e^2 M_{\text{Pl}} (\chi_1^e + \chi_1^\gamma)}{(\chi_1^e - \chi_1^\gamma)^2} \right]^{\frac{1}{3}} & \text{for } \chi_1^\gamma < \chi_1^e \leq 0 \text{ and } \chi_1^\gamma < -3\chi_1^e. \end{cases} \quad (14)$$

The second “new” reaction, photon decay (PD), can be described by

$$\gamma \rightarrow e^+ + e^-. \quad (15)$$

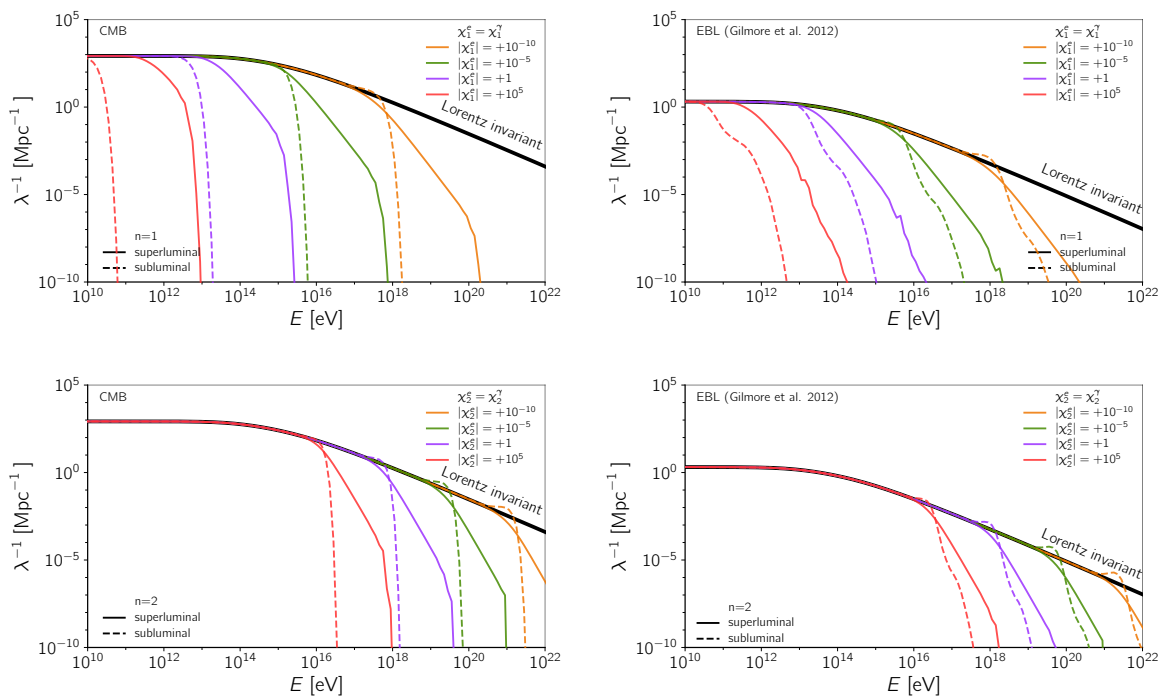


Figure 2. Examples of mean free paths for inverse Compton scattering including LIV calculated according to Eq. (10). The left panel corresponds to the CMB, whereas the right one corresponds to the EBL model from [30]. The upper panels depict the case of first order LIV, whereas the lower ones are for second order LIV. The LIV parameters for each case are indicated in the legend.

This process involves the *spontaneous* transformation of a high-energy photon into an electron-positron pair without interaction with a background photon. Similarly to the VC mechanism, we assume that when the energy of the photon is above a certain threshold for photon decay, it will continually decay into electron-positron pairs until its energy drops below this threshold. Consequently, we again employ a simplified “binary” approach: if the photon’s energy is *above* the threshold, it is reduced to the threshold value, while if the energy is *below* the threshold, photon decay does not occur. This effectively corresponds to a hard cut-off in the photon spectrum, which is a standard approach in this context in the literature [31, 32, 33]. We compute the specific threshold value based on the results presented in [22], which we summarize in the next paragraphs.

We can now determine the minimum threshold energy that a particle has to have in order for VC to take place. This is shown in Fig. 3.

It follows from Fig. 3 that, for the superluminal case (left panel), the value of χ_1^e completely determines the energy threshold of VC regardless of χ_1^γ . For the subluminal case (right panel) the situation is reversed, with $|\chi_1^e|$ exerting little influence on the energy thresholds, which decrease proportionally to $|\chi_1^\gamma|$. Note that the subluminal case does not allow for the region of the parameter space left blank, according to Eq. (14).

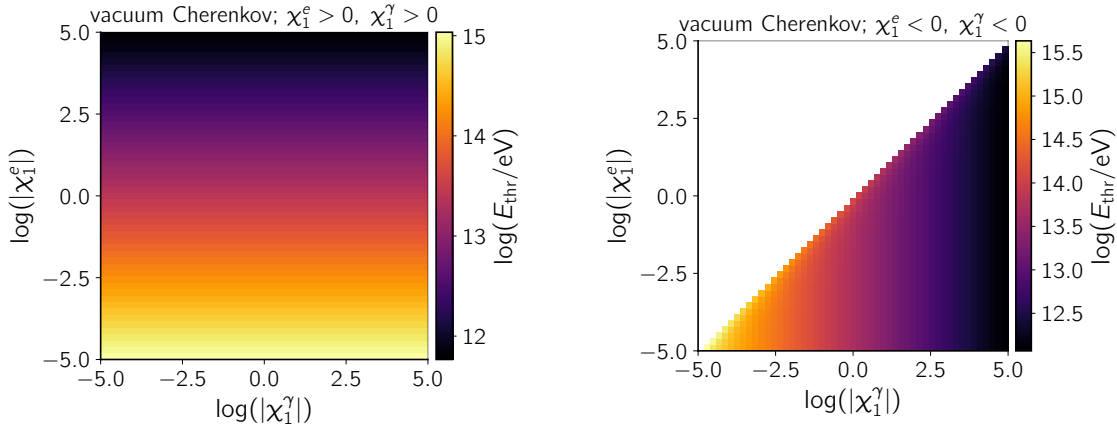


Figure 3. Threshold energy for an electron to emit photons via the vacuum Cherenkov effect, for $n = 1$. The left panel corresponds to the superluminal case ($\chi_1^\gamma > 0$ and $\chi_1^e > 0$), whereas the right one depicts the subluminal scenario ($\chi_1^\gamma < 0$ and $\chi_1^e < 0$).

For $n = 0$ we get the threshold value

$$k_{\text{thr}}^{\text{PD}} = \begin{cases} \frac{2m_e}{(\chi_0^\gamma - \chi_0^e)^{\frac{1}{2}}} & \text{for } \chi_0^\gamma > \chi_0^e, \end{cases} \quad (16)$$

while for $n = 1$ we have

$$k_{\text{thr}}^{\text{PD}} = \begin{cases} \left(\frac{8m_e^2 M_{\text{Pl}}}{2\chi_1^\gamma - \chi_1^e} \right)^{\frac{1}{3}} & \text{for } \chi_1^\gamma \geq 0, \\ \left[-\frac{8m_e^2 M_{\text{Pl}} \chi_1^e}{(\chi_1^e - \chi_1^\gamma)^2} \right]^{\frac{1}{3}} & \text{for } \chi_1^e < \chi_1^\gamma < 0. \end{cases} \quad (17)$$

The threshold energy for PD is shown in Fig. 4.

Fig. 4 indicates that the energy threshold for photon decay in the superluminal case (left panel) decreases as χ_1^e and χ_1^γ jointly increase. The subluminal case (right panel) has a forbidden region, according to Eq. (17), wherein photon decay does not take place. Interestingly, within the allowed region of the parameter space, the energy threshold decreases for large values of $|\chi_1^\gamma|$, as expected, but it decreases for lower $|\chi_1^e|$.

3. Simulations of Electromagnetic Cascades with Lorentz Invariance Violation

To simulate the propagation of gamma-ray-induced electromagnetic cascades, we extend the CRPropa code [34, 35], tapping into the already existing structure of this framework to calculate the relevant kinematics in the presence of LIV [36].

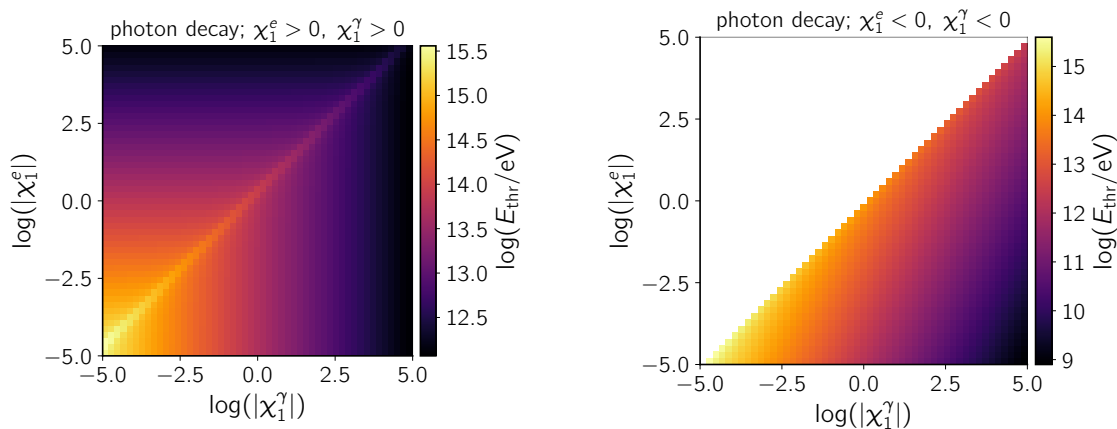


Figure 4. Threshold energy for the photon decay to decay into a pair, for $n = 1$. The left panel corresponds to the superluminal case ($\chi_1^\gamma > 0$ and $\chi_1^e > 0$), whereas the right one depicts the subluminal scenario ($\chi_1^\gamma < 0$ and $\chi_1^e < 0$).

CRPropa[‡] is an advanced framework for simulating the propagation of high and ultra-high-energy messengers. It implements the main interactions relevant for the propagation of each type of messenger, using a Monte Carlo approach. For this work, we modified the existing modules that handle electromagnetic interactions [37], which compute the kinematics of pair production and inverse Compton scattering. These modules make use of the routines provided in CRPropa’s auxiliary repository §. We also implemented new modules for treating vacuum Cherekov and photon decay, taking advantage of the code’s modular structure.

In the following sections we discuss the phenomenology of LIV using simulations obtained with these tools. We select a few scenarios to motivate the discussion, but it is not our goal to compare simulations with observations at this stage. Note that we restrict our analysis to $E < 1$ PeV, considering the substantial computational costs of performing Monte Carlo simulations at higher energies. For this reason, we only present results for the $n = 1$ case, since for $n \geq 2$ there is not significant difference between the Lorentz invariant and the LIV scenarios in the energy range to which we are limited.

We start off by considering the case of LIV affecting the propagation of photons (Sec. 3.1). Then, in Sec. 3.2, we discuss the case of electrons. In Sec. 3.3 we provide comprehensive simulations comprising all effects considered, namely pair production (PP), inverse Compton scattering (ICS), PD, and VC. In Sec. 3.4 we examine the effect of intrinsic source properties on gamma-ray fluxes within the context of LIV.

[‡] <https://crpropa.desy.de/>

[§] <https://github.com/CRPropa/CRPropa3-data>

3.1. Simulations: Photon Propagation

We first consider the propagation of photons only, disregarding any electrons that might have been produced. For the sake of discussion, we first consider a benchmark scenario for two astrophysical sources located at $z = 0.03$ and $z = 0.14$, corresponding to the blazars Mrk 421 and 1ES 0229+200, respectively. The emission spectrum is assumed to be a power-law of the form E^{-2} , with a sharp cut-off at 1 PeV. While this is not necessarily a realistic scenario due to exceedingly high cut-off energy, it does allow us to discuss the main features.

Due to absorption by background cosmological radiation fields, namely the CMB and the EBL, a strong suppression of the flux measured at Earth is expected due to pair-production interactions, at some energy range, depending on the source distance, according to Fig. 1. For instance, any source more distant than ~ 1 Mpc cannot contribute to the gamma-ray flux measured at Earth around ~ 100 TeV. In addition, LIV generally allows for photon decay as well. These two effects, combined, affect the spectrum. This is shown in Fig. 5.

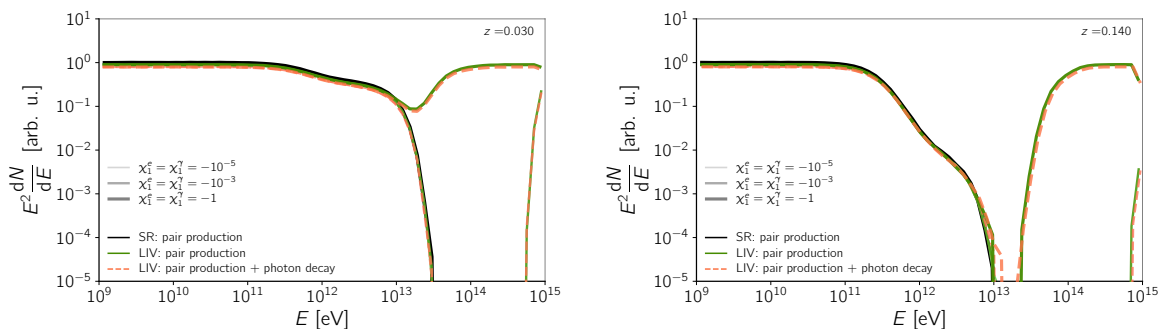


Figure 5. Gamma-ray flux measured at Earth for various scenarios of LIV (coloured lines), for $n = 1$, considering pair production and photon decay. The special-relativistic (SR) scenario is represented by a thick dash-dotted black line. Solid orange lines represent a LIV scenario with PP only, whereas green lines refer to PP and photon decay (PD). Colour gradients and line widths indicate absolute values of LIV coefficients, from thin and lighter (smaller coefficients) to thicker and darker shades (larger coefficients).

It follows immediately from Fig. 5 that while in the Lorentz-invariant scenario no gamma-ray fluxes are expected at energies above $\gtrsim 10$ TeV, in the presence of LIV this is no longer true. An effective change in the transparency of the universe occurs, due to the modification of the interaction thresholds.

3.2. Simulations: Electron Propagation

We now delve into the phenomena influencing the propagation of electrons and positrons. Our approach involves conducting simulations wherein these particles are introduced at the Galactic centre and subsequently traced to Earth. We deliberately disregard any

generated photons within this simulation, to isolate only the relevant processes. It is important to note that a complete assessment would require the inclusion of additional factors, such as deflections caused by the Galactic magnetic field and synchrotron emission. Nevertheless, this simplified scenario effectively serves its purpose: to visually illustrate the alterations in electron fluxes resulting from the breaking of Lorentz symmetry.

To this end, we take the Galactic centre to be our source. We assume it injects electrons. We allow these electrons to propagate to Earth and interact with background photon fields (CMB and EBL) via inverse Compton scattering.

We proceed to examine the impact of vacuum Cherekov on the propagation dynamics. To achieve this, we investigate a scenario similar to that for photons, but this time considering ICS instead of PP, and VC in place of PD. The results are presented in Fig. 6.

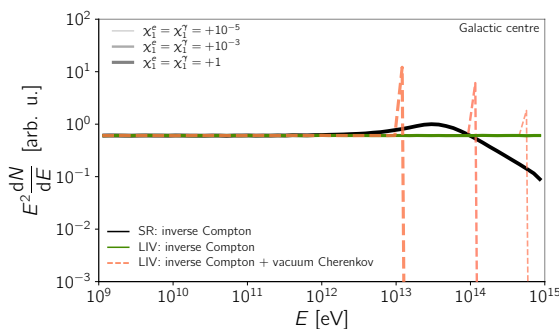


Figure 6. Flux of electrons considering inverse Compton scattering and vacuum Cherekov. The source, in this case, is the Galactic centre. Line styles and colours follow the convention from Fig. 5.

Vacuum Cherekov is undeniably a crucial ingredient for propagation, leading to a noticeable cut-off in the fluxes, as clearly depicted in Fig. 6. The energy at which this effects becomes apparent is determined by the threshold defined in Eq. (14) and illustrated in Fig. 3. For the ICS-only case, there is no suppression due to VC emission, as corroborated by the purple curves. VC, on the other hand, lead to pronounced spectral features around the threshold.

3.3. Simulations: Full LIV Phenomenology

Having isolated each individual effect in the simulations, we now proceed to study a scenario with all relevant phenomenology. We compare the special-relativistic case with the ones including LIV. The results are show in Fig. 7.

The superluminal (purple shades) and subluminal (orange shades) cases of Fig. 7 exhibit very different phenomenological signatures. The latter, in particular, is a clear manifestation of an increased transparency of the universe, thus explaining why a signal is seen at energies above the expected suppression due to the EBL absorption of photons.

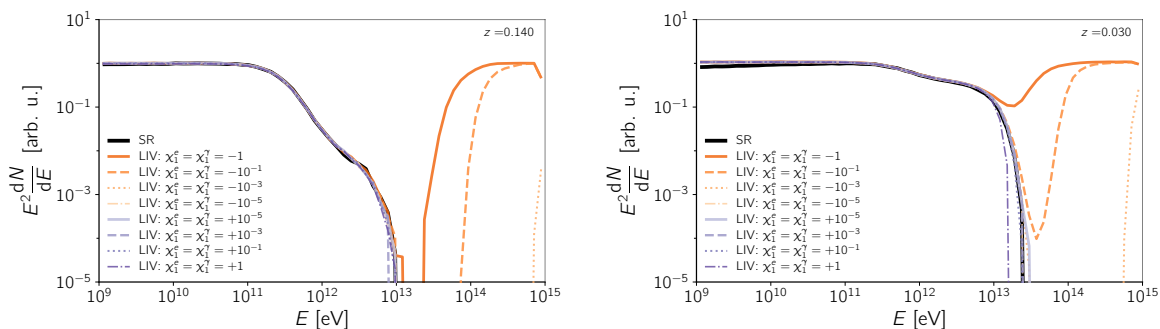


Figure 7. Simulated gamma-ray flux for a source at $z = 0.14$ (left panel) and another at $z = 0.03$ (right panel), considering LIV with $n = 1$. Purple lines correspond to positive LIV coefficients, i.e., the superluminal case, whereas the orange lines refer to the subluminal case (negative values of χ_1), with the darkness of the shades corresponding to the absolute value of the coefficients. The Lorentz-invariant (SR) case is represented by a thick black line.

As expected, a large LIV coefficient (darker line shades) enable gamma rays of very high energies to be observed at Earth, since the changes in the kinematical thresholds would render the universe more transparent. Conversely, a small absolute value of the coefficient (lighter line shades) makes the detection of LIV signatures more challenging, given its similarity to the Lorentz invariant case.

The case for higher-order LIV ($n \geq 2$) leads to much less pronounced features in gamma-ray fluxes. In general, it is hard to separate it from the SR scenario. This could, in principle, change if PD and VC are considered, which we have not done in this in this work.

3.4. Simulations: Effects of the Intrinsic Properties of the Source

The scenarios discussed in the previous sections, while pedagogical, are not realistic. Gamma-ray sources generally emit up to some maximum energy (E_{\max}), determined by an interplay between the maximal energy attainable by their parent cosmic rays (in the case of hadronic sources) and the density of target radiation fields and gas in the surroundings of the emission region. Beyond this energy E_{\max} , the spectrum is suppressed either quickly or more slowly, depending on the exact function describing the suppression.

To understand the impact of the intrinsic source spectrum, we assume an emission of the form

$$\frac{dN}{dE} \propto E^{-\alpha} \exp\left(-\frac{E}{E_{\max}}\right) \quad (18)$$

where α denotes the spectral index. We analyse a couple of cases for the same two sources used in Sec. 3.1. The results are shown in figures 8 and 9.

It is evident from Fig. 8 that for such low values of the LIV coefficient, it is rather challenging to detect any substantial alterations within the same energy range as the

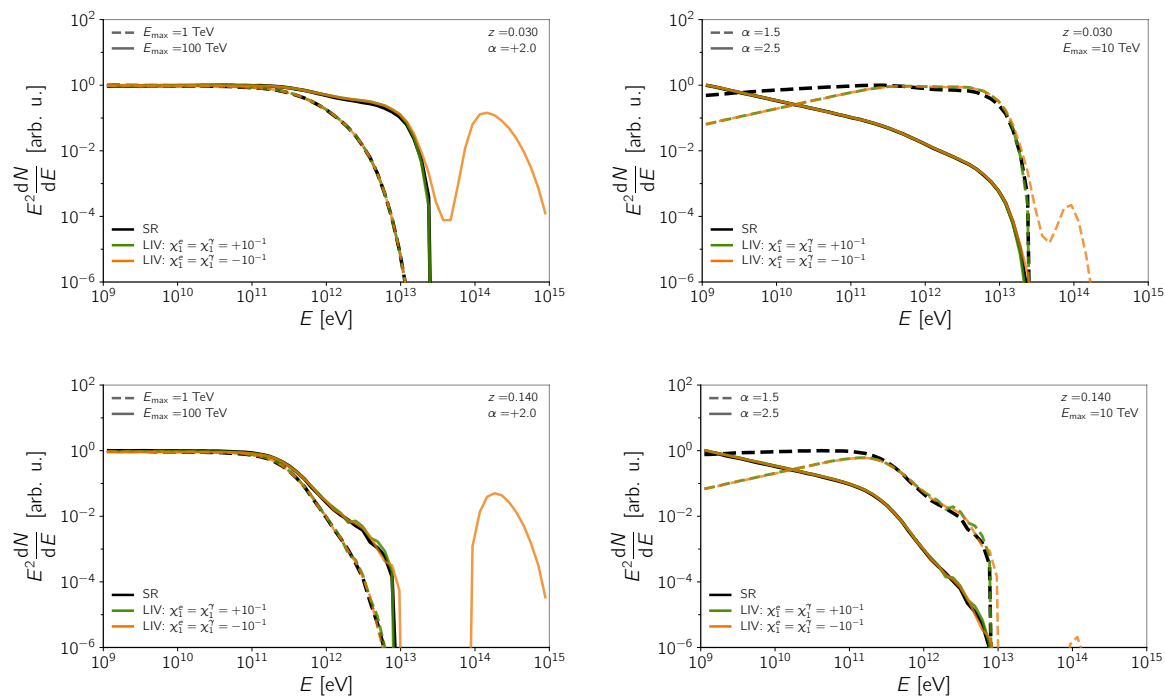


Figure 8. Simulated spectra for two objects, one at $z = 0.03$ (upper panels) and the other at $z = 0.14$ (lower panels). On the left panels the spectral index is fixed to $\alpha = 2$, with the maximal energy (E_{\max}) left to vary. On the right, $E_{\max} = 10$ TeV while α varies. The Lorentz-invariant case is labelled ‘SR’ and represented by a black line. Green and orange lines refer to LIV subluminal and superluminal scenarios, respectively, for LIV coefficients $|\chi_1^e| = |\chi_1^\gamma| = 0.1$.

SR case. The only significant change is a higher-energy bump at $E \gtrsim 100$ TeV for the subluminal case. Nevertheless, this is only visible for larger values of E_{\max} , as supported by the panels on the left. Similarly, lower spectral indices also favour the detectability of LIV effects for the cases studied. If the LIV effect is stronger, as illustrated in fig 9, LIV signatures are more easily detectable, even at sub-TeV energies. This is particularly relevant for the harder spectra, shown on the right panels, and it can be partly attributed to the absence of the photon component generated by inverse Compton scattering of electrons produced by primary photons that did not interact. In fact, this can be understood in terms of the strong suppression due to VC, shown in Fig. 6.

The source distance also plays a role in determining the fluxes to be measured at Earth. While this is not really visible for the smaller LIV coefficients from Fig. 8, it can be seen in Fig. 9, by comparing the upper and the lower rows.

4. Discussion

It is important to emphasise that the phenomenon of Lorentz invariance violation extends beyond mere alterations of interaction thresholds, which have dominated the works on the topic so far. Within the confines of a single effective field theory,

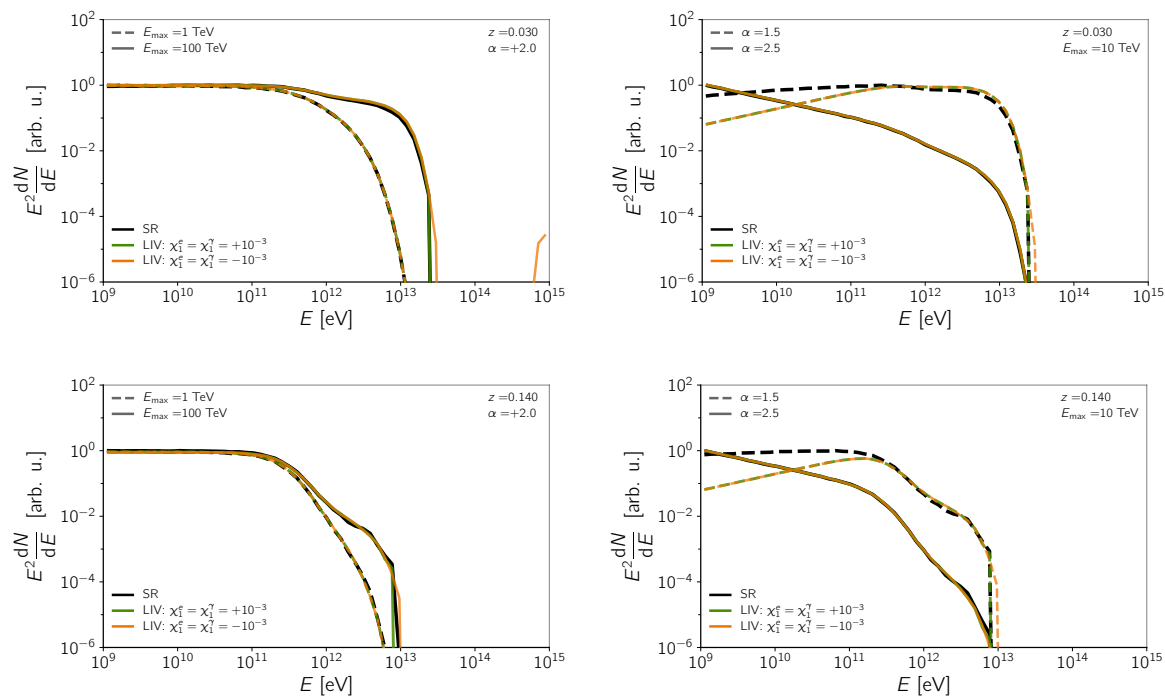


Figure 9. Same as Fig. 8 for LIV coefficients $|\chi_1^e| = |\chi_1^\gamma| = 10$.

novel processes that are typically prohibited under a Lorentz-invariant scenario start to surface. Noteworthy examples are photon decay ($\gamma \rightarrow e^+ + e^-$), photon splitting ($\gamma \rightarrow \gamma + \gamma + \gamma$), and vacuum Cherenkov radiation ($e^\pm \rightarrow e^\pm + \gamma$) [22, 38]. Prior investigations using TeV observations of astrophysical objects, such as the Crab Nebula, have placed constraints on LIV in the quantum electrodynamics (QED) sector through searches for these effects [39, 40].

It should be noted here that the aforementioned “binary” treatment of these new reactions (in this paper specifically photon decay and the vacuum Cherenkov effect) is a very simplified approach. Using a more sophisticated treatment, taking into account the full spectrum of the corresponding secondaries, this might change the overall observed spectrum. However, we chose the simplification, on the one hand, due to the fact that a full treatment involves non-trivial quantum-electrodynamical calculations which are beyond the scope of the phenomenological approach of the present paper. On the other hand, VC and PD usually occur on length scales much shorter than ICS and PP, such that the particles undergoing the latter two reactions are already the result of the two former reactions, and therefore the effects may, at least to some degree as a compromise, be treated separately.

One interesting result that is not often discussed in the literature is the crucial role played by the source intrinsic spectrum in determining the detectability of LIV effects. Our results indicate that either a large maximal energy (E_{\max}) or a harder spectrum (smaller α) enhance the detectability of the signals. Astrophysical sources whose bulk integrated energy lies below \sim TeV are not suitable objects for LIV studies, specially if

their spectrum is soft ($\alpha \gtrsim 2$). This is not surprising, given that a pronounced cascade contribution is required for interactions to occur and thus to enable LIV studies. Several types of objects satisfy these criteria, with certain types of blazars and gamma-ray bursts (GRBs) arguably being the most relevant ones [41, 19, 42, 43]. Extreme blazars, in particular, tend to have a harder spectrum and often their emission is detected up to multi-TeV energies. Nevertheless, it is important to note that intrinsic source properties also depend on propagation details, like intervening magnetic fields, as shown in [44].

It can be seen here that several cases presented above contain some kind of flux suppression, which might overlap with the flux suppression due to the interaction of cascade electrons with magnetic fields [27] (or with the intergalactic medium [45]). In fact, the other two phenomenological consequences of magnetic fields onto the electromagnetic cascade, namely the time delay and the seeming broadening of a point source, can also result from LIV, making it difficult to distinguish the two effects. In particular, this means that if one takes LIV into account, the limits previously derived for intergalactic magnetic fields might be altered.

Several of the cases presented in this work result in a different kind of spectral feature, namely a distinct peak at high energies, which is separated from the rest of the spectrum by a gap (see, for example, the bottom left panel of Fig. 8). If such a feature is observed, one might be tempted to conclude that the two separated parts of the spectrum stem from two different processes/regions at the source emitting particles in two different energy bands or an additional radiation field absorbing photons. Our findings, however, allow for the possibility that it is simply a propagation effect, just with LIV included.

Other factors would affect the results presented. For instance, the EBL model determines the interaction rates of pair production (see Fig. 1). The effect of the EBL in the presence of LIV would not qualitatively differ from the Lorentz-invariant case.

Intergalactic magnetic fields (IGMFs) could affect the charged component of the cascade, potentially altering the energy spectra expected at Earth [27]. In fact, this could greatly impact gamma-ray-based estimates of IGMFs (e.g., [46, 47, 48, 49, 50]). Similarly, the interplay between the geometry of emission and IGMFs could change spectral and angular signatures of gamma rays from misaligned jetted sources [51].

We have performed this investigation only for electromagnetic interactions, but analogous signatures are expected for other types of travelling messengers, like UHECRs. In particular, the GZK effect due to the interaction of energetic protons with the CMB, if it occurs, could be substantially altered in the presence of LIV, as studied in [52, 53, 54, 55].

5. Conclusions and Outlook

In this study, we have conducted detailed Monte Carlo simulations to investigate the impact of Lorentz invariance violation on gamma-ray propagation. In addition to the conventional propagation effects, such as pair production and inverse Compton

scattering, we have also incorporated two phenomena stemming from the breaking of Lorentz symmetry: photon decay and vacuum Cherekov. To the best of our knowledge, this work represents the first and most detailed attempt to model the development of electromagnetic cascades in the intergalactic medium in the presence of LIV.

Our findings underscore the complex interplay among several types of effects, revealing that, combined, they can lead to strong deviations in the expected flux of extraterrestrial gamma rays reaching Earth. The main phenomenological consequences include a change in the transparency of the universe to high-energy gamma rays, as well as characteristic spectral features that impact the measured fluxes.

One of our most remarkable findings highlights the role of the often-overlooked inverse Compton scattering, which can exert a substantial influence on gamma-ray fluxes in some cases. Incorporating ICS into most analyses is essential due to its potential to affect fluxes, especially in the GeV–TeV band. This is a consequence from the intricate interplay between excess (or deficit) of photons at high energies, relative to the predictions of SR, and its impact on the generation of secondary photons through ICS. Although the effect may be modest in magnitude, it evidently compromises the interpretation of observations and ought to be taken into account, even if only to assess its (in)significance.

Also striking is the fact that a combined consideration of ICS and VC could, in certain scenarios, lead to striking signatures at *lower energies*.

In the future, we envision expanding our analysis in several directions. One avenue of exploration involves refining our treatments of photon decay and vacuum Cherekov, which currently are done only for LIV of order $n = 0$ and $n = 1$, in particular by using a complete quantumelectrodynamics treatment, such as, for example, the one presented in [56] for $n = 2$. We also intend to generalise the LIV formalism to allow superposition of order (multiple values of n acting together). Finally, we intend to include effects of magnetic fields to understand how they can affect the charged leptonic component of electromagnetic cascades.

Furthermore, we also plan to extend our analysis to a proper treatment of the secondaries resulting from the new reactions made possible by LIV. As described in Sec. 2.2, in this work we used a very simplified binary approach by just reducing the energy and momentum of the corresponding particle above the threshold to the threshold value. However, preliminary results of further investigations show that the emission of secondaries in both cases is a process with complicated kinematics which means that the energy distribution between them might significantly deviate from the Lorentz-invariant case, possibly compromising the co-linear approximation employed, wherein the momenta of highly relativistic secondaries are parallel to the parent’s momentum. Depending on the value of the LIV parameter, this can therefore result in significant observational features.

Data Availability Statement

The code used for the simulations in this manuscript is being prepared to be made public. In the meantime, it can be made available upon reasonable request. The data that support the findings of this study are available upon reasonable request from the authors.

Acknowledgements

The work of AS is supported by the Russian Science Foundation under grant no. 22-11-00063. RAB is funded by the “la Caixa” Foundation (ID 100010434) and the European Union’s Horizon 2020 research and innovation program under the Marie Skłodowska-Curie grant agreement No 847648, fellowship code LCF/BQ/PI21/11830030, and by the grants PID2021-125331NB-I00 and CEX2020-001007-S, both funded by MCIN/AEI/10.13039/501100011033 and by “ERDF A way of making Europe”.

References

- [1] Gaillard M K, Grannis P D and Sciulli F J 1999 *Rev. Mod. Phys.* **71** S96–S111 (*Preprint hep-ph/9812285*)
- [2] Cottingham W T and Greenwood D A 2023 *An Introduction to the Standard Model of Particle Physics* (Cambridge University Press)
- [3] Golling T *et al.* 2017 *CERN Yellow Rep.* **3** 441–634 (*Preprint 1606.00947*)
- [4] Addazi A *et al.* 2022 *Prog. Part. Nucl. Phys.* **125** 103948 (*Preprint 2111.05659*)
- [5] Mattingly D 2005 *Liv. Rev. Rel.* **8** 5 (*Preprint gr-qc/0502097*)
- [6] Bietenholz W 2011 *Phys. Rep.* **505** 145–185 (*Preprint 0806.3713*)
- [7] Saveliev A, Maccione L and Sigl G 2011 *J. Cosmol. Astropart. Phys.* **2011** 046 (*Preprint 1101.2903*)
- [8] Galaverni M and Sigl G 2008 *Phys. Rev. D* **78** 063003 (*Preprint 0807.1210*)
- [9] Martínez-Huerta H, Lang R G and de Souza V 2020 *Symmetry* **12** 1232
- [10] Colladay D and Kostelecký V A 1998 *Phys. Rev. D* **58** 116002 (*Preprint hep-ph/9809521*)
- [11] Alfaro J 2005 *Phys. Rev. Lett.* **94** 221302 (*Preprint hep-th/0412295*)
- [12] Collins J, Perez A, Sudarsky D, Urrutia L and Vucetich H 2004 *Phys. Rev. Lett.* **93** 191301 (*Preprint gr-qc/0403053*)
- [13] Sotiriou T P, Visser M and Weinfurtner S 2009 *J. High Energy Phys.* **10** 033 (*Preprint 0905.2798*)
- [14] Reyes C M, Ossandon S and Reyes C 2015 *Phys. Lett. B* **746** 190–193 (*Preprint 1409.0508*)
- [15] Amelino-Camelia G 2002 *Nature* **418** 34–35 (*Preprint gr-qc/0207049*)
- [16] Morais P H, Lobo I P, Pfeifer C, Alves Batista R and Bezerra V B 2024 *Phys. Lett. B* **848** 138380 (*Preprint 2308.03716*)
- [17] Amelino-Camelia G, Ellis J R, Mavromatos N E, Nanopoulos D V and Sarkar S 1998 *Nature* **393** 763–765 (*Preprint astro-ph/9712103*)
- [18] Ellis J R, AMD Mavromatos N E, Nanopoulos D V, Sakharov A S and Sarkisyan E K G 2006 *Astropart. Phys.* **25** 402–411 [Erratum: *Astropart. Phys.* 29, 158–159 (2008)] (*Preprint 0712.2781*)
- [19] Ellis J and Mavromatos N E 2013 *Astropart. Phys.* **43** 50–55 (*Preprint 1111.1178*)
- [20] Ellis J, Konoplich R, Mavromatos N E, Nguyen L, Sakharov A S and Sarkisyan-Grinbaum E K 2019 *Phys. Rev. D* **99** 083009 (*Preprint 1807.00189*)
- [21] Jacob U and Piran T 2008 *J. Cosmol. Astropart. Phys.* **2008** 031 (*Preprint 0712.2170*)

- [22] Jacobson T, Liberati S and Mattingly D 2003 *Phys. Rev. D* **67** 124011 (*Preprint hep-ph/0209264*)
- [23] Mattingly D, Jacobson T and Liberati S 2003 *Phys. Rev. D* **67** 124012 (*Preprint hep-ph/0211466*)
- [24] Bertolami O 2003 *Lect. Notes Phys.* **633** 96–102 (*Preprint hep-ph/0301191*)
- [25] Baccetti V, Tate K and Visser M 2012 *J. High Energy Phys.* **03** 087 (*Preprint 1111.6340*)
- [26] Martínez-Huerta H, Lang R G and de Souza V 2018 *Proc. of Science* **BHCB2018** 010 (*Preprint 1901.03205*)
- [27] Alves Batista R and Saveliev A 2021 *Universe* **7** 223 (*Preprint 2105.12020*)
- [28] Vankov H and Stanev T 2002 *Phys. Lett. B* **538** 251–256 (*Preprint astro-ph/0202388*)
- [29] Terzić T, Kerszberg D and Strišković J 2021 *Universe* **7** 345 (*Preprint 2109.09072*)
- [30] Gilmore R C, Somerville R S, Primack J R and Domínguez A 2012 *Mon. Not. R. Astron. Soc.* **422** 3189 (*Preprint 1104.0671*)
- [31] Albert A *et al.* (HAWC) 2020 *Phys. Rev. Lett.* **124** 131101 (*Preprint 1911.08070*)
- [32] Chen L, Xiong Z, Li C, Chen S Z and He H H 2021 *Chin. Phys. C* **45** 105105 (*Preprint 2105.07927*)
- [33] Cao Z *et al.* (LHAASO) 2022 *Phys. Rev. Lett.* **128** 051102 (*Preprint 2106.12350*)
- [34] Alves Batista R, Dundovic A, Erdmann M, Kampert K H, Kuempel D, Müller G, Sigl G, van Vliet A, Walz D and Winchen T 2016 *J. Cosmol. Astropart. Phys.* **5** 038 (*Preprint 1603.07142*)
- [35] Alves Batista R *et al.* 2022 *J. Cosmol. Astropart. Phys.* **09** 035 (*Preprint 2208.00107*)
- [36] Saveliev A and Alves Batista R 2023 *PoS ICRC2023* 903 (*Preprint 2307.11421*)
- [37] Heiter C, Kuempel D, Walz D and Erdmann M 2018 *Astropart. Phys.* **102** 39–50 (*Preprint 1710.11406*)
- [38] Gelmini G, Nussinov S and Yaguna C E 2005 *J. Cosmol. Astropart. Phys.* **2005** 012 (*Preprint hep-ph/0503130*)
- [39] Astapov K, Kirpichnikov D and Satunin P 2019 *J. Cosmol. Astropart. Phys.* **2019** 054 (*Preprint 1903.08464*)
- [40] Satunin P 2019 *Eur. Phys. J. C* **79** 1011 (*Preprint 1906.08221*)
- [41] Bertolami O and Carvalho C S 2000 *Phys. Rev. D* **61** 103002 (*Preprint gr-qc/9912117*)
- [42] Vasileiou V, Jacholkowska A, Piron F, Bolmont J, Couturier C, Granot J, Stecker F W, Cohen-Tanugi J and Longo F 2013 *Phys. Rev. D* **87** 122001 (*Preprint 1305.3463*)
- [43] Lang R G, Martínez-Huerta H and de Souza V 2019 *Phys. Rev. D* **99** 043015 (*Preprint 1810.13215*)
- [44] Saveliev A and Alves Batista R 2021 *Mon. Not. R. Astron. Soc.* **500** 2188–2195 (*Preprint 2009.09772*)
- [45] Alves Batista R, Saveliev A and de Gouveia Dal Pino E M 2019 *Mon. Not. R. Astron. Soc.* **489** 3836–3849 (*Preprint 1904.13345*)
- [46] Neronov A and Vovk I 2010 *Science* **328** 73–75 (*Preprint 1006.3504*) URL <http://www.sciencemag.org/content/328/5974/73.abstract>
- [47] Tavecchio F, Ghisellini G, Foschini L, Bonnoli G, Ghirlanda G and Coppi P 2010 *Mon. Not. R. Astron. Soc.* **406** L70–L74 (*Preprint 1004.1329*)
- [48] Finke J, Reyes L and Georganopoulos M (Fermi-LAT) 2012 *eConf* **C121028** 365 (*Preprint 1303.5093*)
- [49] Ackermann M *et al.* (Fermi-LAT) 2018 *Astrophys. J. Suppl.* **237** 32 (*Preprint 1804.08035*)
- [50] Alves Batista R and Saveliev A 2020 *Astrophys. J. Lett.* **902** L11 (*Preprint 2009.12161*)
- [51] Neronov A, Semikoz D, Kachelrieß M, Ostapchenko S and Elyiv E 2010 *Astrophys. J. Lett.* **719** L130 (*Preprint 1002.4981*)
- [52] Scully S T and Stecker F W 2009 *Astropart. Phys.* **31** 220–225 (*Preprint 0811.2230*)
- [53] Maccione L, Taylor A M, Mattingly D M and Liberati S 2009 *J. Cosmol. Astropart. Phys.* **04** 022 (*Preprint 0902.1756*)
- [54] Stecker F W and Scully S T 2009 *New J. Phys.* **11** 085003 (*Preprint 0906.1735*)
- [55] Torri M D C, Caccianiga L, di Matteo A, Maino A and Miramonti L 2020 *Symmetry* **12** 1961 (*Preprint 2110.09900*)
- [56] Rubtsov G, Satunin P and Sibiryakov S 2012 *Phys. Rev. D* **86** 085012 (*Preprint 1204.5782*)